Applied Catalysis A: General 492 (2015) 184–189

Contents lists available at ScienceDirect

Applied Catalysis A: General

journal homepage: www.elsevier.com/locate/apcata

Ag nanoparticle-immobilized cellulose nanofibril films for environmental conservation

Bendi Ramaraju[a], Toyoko Imae[a,b,*], Addisu Getachew Destaye[b]

[a] Graduate Institute of Applied Science and Technology, National Taiwan University of Science and Technology, 43 Section 4, Keelung Road, Taipei 10607, Taiwan

[b] Department of Chemical Engineering, National Taiwan University of Science and Technology, 43 Section 4, Keelung Road, Taipei 10607, Taiwan

ARTICLE INFO

Article history:
Received 5 September 2014
Received in revised form
20 December 2014
Accepted 24 December 2014
Available online 31 December 2014

Keywords:
Cellulose nanofiber
Dendrimer
Catalysis
Antibacterial activity
Nanocomposite film

ABSTRACT

A facile method was developed to prepare biodegradable nanocomposite films. Ag nanoparticles stabilized by an NH_2-terminated fourth generation poly(amido amine) dendrimer (DENAgNPs) were covalently immobilized on 2,2,6,6-tetramethylpiperidine-1-oxyl radical-oxidized nanofibrillated cellulose (NFC) by using a condensing agent for amide bond formation between NFC and DENAgNPs. Subsequently, the films with different concentrations of DENAgNPs were prepared by filtrating DENAgNPs-NFC suspensions on filter membranes, and the dried films were characterized. As-prepared films possessed the high catalytic efficiency to decoloration of Rhodamine B in water and the excellent antibacterial performance against both Gram-positive and Gram-negative bacteria on agar plates. Thus, this novel concept of film-type nanocomposite reactor demonstrates that it is possible to prepare inexpensive catalytic and bactericidal-active films with good selectivity by easy prospective approach for realizing the environmental conservation and innovation.

1. Introduction

Numerous classes of pigments are widely used in many industries and lead to severe contamination in surface water and groundwater from the release of toxic and colored effluents [1,2]. Meanwhile, various microorganisms coexist with human body and living environments, and their rapid and uncontrolled breeding can result in some serious problems like foul smell and health disturbance [3,4]. It is, therefore, essential to develop an eco-friendly and effective materials having catalytic properties for degradation of organic compounds and antibacterial properties, and it is of great significance to minimize, in such a way, the causes of hazards in the aquatic environments and human lives. The use of nanocomposites for the protection from carcinogenic, toxic dye molecules and microbial contamination may provide solutions for the challenges faced by the health care system in this century.

Parallel to eco-friendly criteria, cellulose is the most abundant natural polymer and an almost inexhaustible raw material for the fabrication of functional materials with various high performances [5,6]. As a chemical raw material, cellulose has been used for long periods [7]. Wood is essentially a network of cellulose fiber held together by a matrix of lignin. Wood pulp is produced through a variety of processes, all of which break down and wash away the lignin. A typical cellulose wood fiber, microfibrillated cellulose (MFC), is of only tens of micrometer wide and about a millimeter long. Meanwhile, the cellulose with carboxyl functional groups has been found to be an excellent eco-friendly matrix stabilizing metal nanoparticles [8]. As a novel approach, 2,2,6,6-tetramethylpiperidine-1-oxyl (TEMPO)-mediated oxidation introduces carboxylate and aldehyde functional groups into cellulosic materials and makes MFC to nanofibrillated cellulose (NFC) in an aqueous medium, at mild conditions of room temperature and atmospheric pressure, and at pH 10–11.

NFCs reveal unique physicochemical behaviors and possess mechanical properties that are superior to bulk cellulose [9]. NFCs have gained considerable interests as an abundant biocompatible material with potential applications in a wide variety of fields ranging from tissue scaffolds to flexible electronics. Cellulose nanomaterials have previously been studied as reinforcement materials for various polymer matrices but they have recently been integrated into different applications [10–13]. NFCs have been used as a soft matrix to accommodate inorganic fillers (like metal nanoparticles) to produce inorganic–organic composites that bring together

* Corresponding author at: Graduate Institute of Applied Science and Technology, National Taiwan University of Science and Technology, 43 Section 4, Keelung Road, Taipei 10607, Taiwan. Tel.: +886 2 2730 3627; fax: +886 2 2730 3627.
E-mail address: imae@mail.ntust.edu.tw (T. Imae).

http://dx.doi.org/10.1016/j.apcata.2014.12.045
0926-860X/

the intrinsic functionalities of the fillers and the bio-interface properties of cellulose fibers [14,15].

Nanostructured catalysts can effectively eliminate the organic pollutants and present antibacterial performance [16–18]. However, secondary pollution is one of the problems limiting the widespread applications of the nanostructured catalysts [19]. In other words, a serious issue is created due to the difficulty of separating the utilized nanostructured catalysts from the treated water, especially in the case of large-scale processes [20]. In this regard, to avoid secondary pollution, we have reported the embedding of Cu nanoparticles into the cellulose nanofiber film and utilized it for 4-nitrophenol reduction [21].

Herein, Ag nanoparticles (AgNPs) protected by poly(amido amine) (PAMAM) dendrimer (DENAgNPs) were synthesized at the condition, where the ratio of metal precursor to amine terminal group of PAMAM dendrimer was optimized so as to provide the stably dispersed AgNPs [22]. Then DENAgNPs were covalently immobilized on NFC by means of the chemical reaction, which is well known to form an amide bond [23]. Finally we focused to prepare films from aqueous suspensions of DENAgNPs-NFC nanocomposites by filtration. The formation of DENAgNPs-NFC films was characterized and confirmed via conventional analytical methodologies. This film-type novel material showed both catalytic and anti-bacterial activity. The mechanisms of decoloration and anti-bacterial activity were also shown in schematically.

2. Experimental

2.1. Materials

Silver nitrate (99.99%), methanol (99.8%), N-hydroxysuccinimide (NHS), 1-ethyl-3-(3-dimethylaminopropyl)-carbodiimide (EDC), fourth generation (G4) PAMAM dendrimer with 64 NH_2 terminals and Rhodamine B were purchased from Aldrich Chemical Co. Other reagents and solvents were purchased from Acros Organics. All of these chemicals were used without modification. Ultrapure water was used throughout all experiments.

Since the detailed preparation of NFC used in the present study is described elsewhere [21], a brief description is given here. MFC was prepared by removal of wax and lignin from the sliced wood (softwood) by means of chemical treatment. MFC suspended in an aqueous solution of TEMPO and sodium bromide was oxidized by slowly pouring sodium hypochlorite (13 vol%) under constant stirring at room temperature and pH 10 throughout the reaction. Thus-obtained NFC was rinsed thoroughly with water, centrifuged and stored in the wet state.

2.2. Fabrication of DENAgNPs-NFC composite films

The synthesis procedure at optimum ratio (0.01:1) of Ag^+:NH_2 group (in dendrimer) for preparation of small size of stable metal nanoparticles was followed the previous report [22]. The formation of nanoparticles was confirmed by the observation of a surface plasmon resonance band at 443 nm in an ultraviolet (UV)–visible absorption spectrum, while this band was absent for an $AgNO_3$ solution (Fig. S1 in Appendix A). All AgNPs were almost spherical, and its average size was 6.2 nm, as apparent from transmission electron microscopic (TEM) results in Fig. S2 in Appendix A.

The covalent crosslinking between NFC and DENAgNPs was done based on the well-known amidation reaction [23–25]. NFC in water (1 wt%) was reacted with equimolar coupling reagents, EDC and NHS to form a stable NHS-carboxylated NFC. After that, an aqueous DENAgNPs solution was added to accomplish the formation of DENAgNPs-NFC. The existence of DENAgNPs in DENAgNPs-NFC was confirmed by a plasmon band in comparison with spectra of NFC and DENAgNPs, as shown in Fig. S3 in Appendix A. The schematic representation of the formation of DENAgNPs-NFC nanocomposites is illustrated in Fig. 1.

The DENAgNPs-NFC films were prepared by the filtration of aqueous DENAgNPs-NFC suspensions on the cellulose acetate filter membrane with 47 mm diameter and 0.2 μm pore size. Then the DENAgNPs-NFC films were separated from the filter membrane. By way of comparison, films with different amount of DENAgNPs were prepared by varying an addition of an aqueous DENAgNPs solution in the reaction solution like 0 mL, 1 mL, 2 mL or 3 mL, and they were named as Film A, Film B, Film C and Film D, respectively. If the addition was increased more than 3 mL, the aggregation or precipitation of DENAgNPs in the NFC suspension was observed.

2.3. Characterization

UV–visible absorption spectra were recorded on a Jasco V-670 spectrophotometer. TEM observation was carried out on a Hitachi H-7000 instrument equipped with a CCD camera, operating at a voltage of 100 kV. Specimens were prepared by spreading a small drop (2 μL) of diluted suspensions onto standard carbon-coated copper grids and drying. Fourier transform-infrared (FT-IR) absorption spectra were recorded on a Nicolet 6700 spectrometer. X-ray photoelectron spectroscopic (XPS) measurement was carried out on a VG Scientific Model ESCA Lab 250 spectrometer. Thermogravimetric analysis (TGA) was performed using a TA instrument Q500 under nitrogen flow at a heating rate of 10 °C/min.

2.4. Catalytic and antibacterial reactions

Rhodamine B was used as a model organic dye to evaluate the catalytic activity of DENAgNPs-NFC films. The film was immersed into an aqueous Rhodamine B solution (10 mg/L, 100 mL), and an aqueous $NaBH_4$ solution (0.1 M, 1 mL) was added to initiate the decoloration reaction. During keeping in darkness, the pink color of Rhodamine B gradually vanished with catalytic reduction of dye. The efficiency of the catalysis was monitored by UV–visible absorption spectrometry.

Antibacterial activities were investigated for *Escherichia coli* (*E. coli*) and *Staphylococcus aureus* (*S. aureus*) as models for Gram-negative and Gram-positive bacteria, respectively. The activity was evaluated by the size of the inhibited clear zone on the disc diffusion method. The microorganisms were cultivated in tubes containing 5 mL of sterile nutrients: Luria–Bertani (LB) for *E. coli* and tryptic soy broth (TSB) for *S. aureus* were incubated for 24 h at 37 °C. The bacteria cells were diluted to a final concentration of OD_{600} = 0.05 and placed onto LB and TSB agar plates. Sample membranes were cut into disk shape of 0.5 cm diameter and UV-sterilized for 20 min. Then, the disks were placed onto the agar plates with the bacteria culture, and the plates were incubated for 24 h at 37 °C. Clear zones of inhibition formed around the disks were measured and compared with control samples.

3. Results and discussion

3.1. Characterization of DENAgNPs-NFC films

Due to the TEMPO oxidation treatment, primary hydroxyl groups at the C6 position of cellulose molecules are oxidized to sodium carboxylate groups (COONa). Sodium ions, counter ions of oxidized cellulose, can be exchanged with metal ions to provide cellulose–metal complex in the aqueous metal salt solution [21]. However, the active sites are limited and fewer amounts of metal particles are only loaded on the NFC networks. Hence, the present study focused to combine AgNPs-encapsulated PAMAM dendrimer

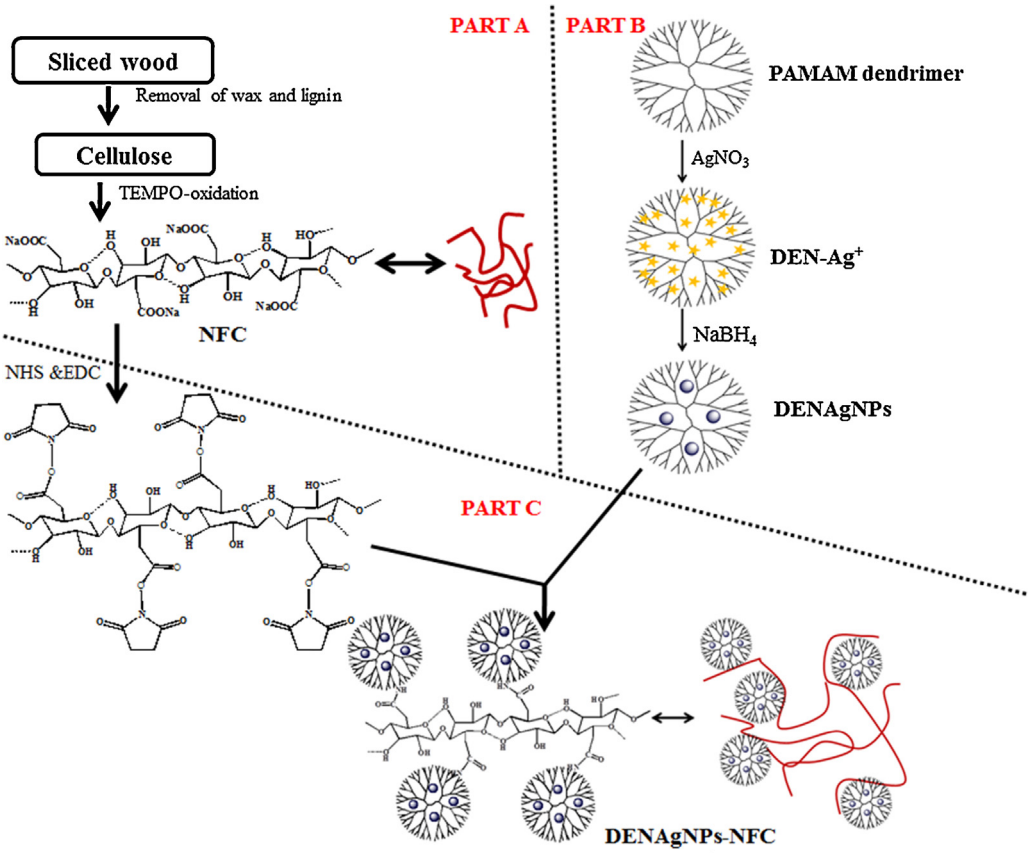

Fig. 1. Schematic illustration of amidation reaction between NFC and DENAgNPs.

(DENAgNPs) on cellulose through amidation reaction [23–25]. Fourth generation (G4) PAMAM dendrimer is a polymer, which possesses 62 reactive tertiary amine groups in its interior, and this structural character makes PAMAM dendrimer the potential capping agent of many metal nanoparticles [22]. Moreover, it was experimentally provided from ultraviolet (UV)–visible absorption spectra for the suspension of the film in water and its filtrate (Fig. S4 in Appendix A) that the DENAgNPs-NFC film displayed no elution of AgNPs from the film, different from non-amidated composite film. Visual observation of the nanocomposite films (Fig. 2a) with different amount of DENAgNPs showed a primary evidence for the existence of the DENAgNPs in the nanocomposite films. The color change clearly indicated the increasing concentration of DENAgNPs from Film B to Film D. Those films were analyzed by UV–visible absorption spectroscopy as represented in Fig. 2b. It was clearly elucidated that the surface plasmon resonance band of AgNPs was at 418.2 nm, and its absorbance increased with increasing the concentration of AgNPs on films.

The Fourier transform-infrared (FT-IR) absorption spectra of NFC (Film A) and DENAgNPs-NFC nanocomposite (Film B) films are shown in Fig. 3 and Fig. S5 in Appendix A. The absorption spectrum of NFC exhibited characteristic absorption bands for cellulose, such as OH stretching at 3354 cm^{-1}, CH stretching at 2891 cm^{-1}, OH and CH bending as well as C—C and C—O stretching at 1380, 1317, and 1256 cm^{-1}, and C—O—C skeletal at 1055 cm^{-1} [26,27]. Bands at 1600 and 1420 cm^{-1} were assigned to carboxylate stretching [28]. The spectrum of DENAgNPs-NFC nanocomposite films showed successful amidation grafting of DENAgNPs on NFC through characteristic absorption bands of PAMAM dendrimer like NH_2 stretching at 3094 cm^{-1} and amide I and II at 1657 cm^{-1} and 1559 cm^{-1}, respectively [29]. The bands at 2936 and 2845 cm^{-1} were assigned to CH_2 stretching and a band at 1456 cm^{-1} was attributed to CH_2 bending mode [30,31].

Thermogravimetric analyses (TGA) of NFC and DENAgNPs-NFC films were carried out under nitrogen atmosphere to evaluate their degradation profile and thermal stability. Both TG curves (see Fig. 4) showed an initial small drop between 50 and 150 °C, which

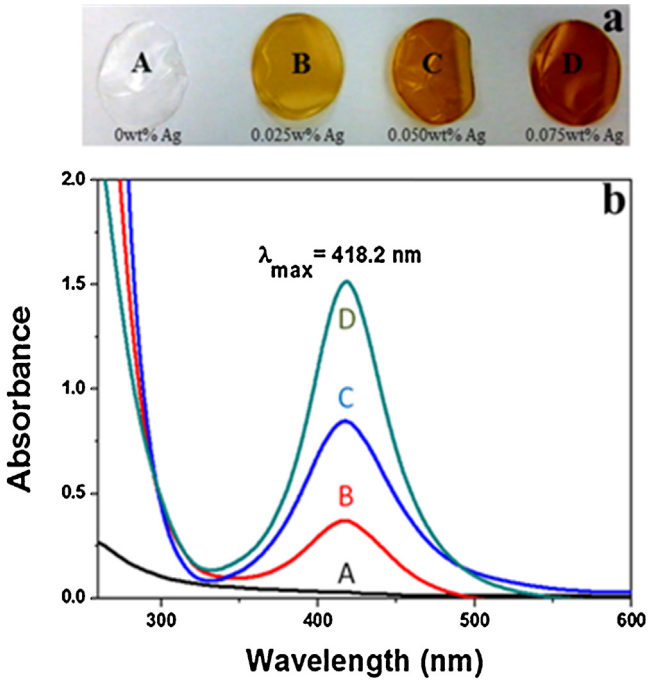

Fig. 2. (a) Visual observation and (b) UV–visible absorption spectra of NFC (A) and DENAgNPs-NFC (B–D) films.

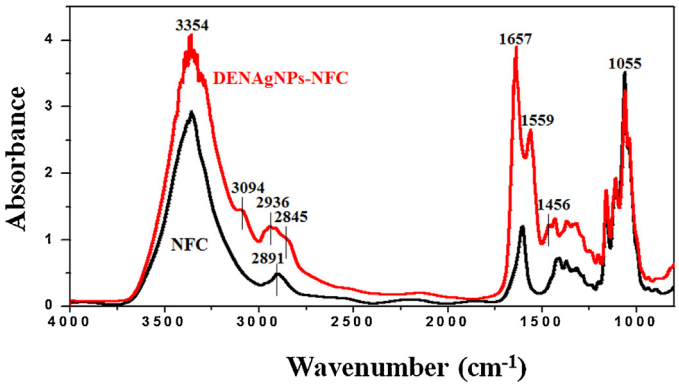

Fig. 3. FT-IR absorption spectra of NFC (Film A) and DENAgNPs-NFC (Film B) films.

corresponded to a weight loss of approximately 17% for NFC film (Film A) and 8% for DENAgNPs-NFC film (Film B). This indicates the loss of adsorbed moisture on both films including chemisorbed and/or hydrogen bonded water. Thermal degradation started at approximately 200 °C and 225 °C for NFC and NFC-DENAgNPs films, respectively. Thus, the formation of amide bond at C6 carboxyl group led to the small increase in the thermal degradation temperature of NFC.

The elemental composition of DENAgNPs-NFC film was compared with NFC film by X-ray photoelectron spectroscopy (XPS). As shown in Fig. 5, compared with the NFC film (Film A), new peaks corresponding to N1s (400.0 eV) and Ag3d (368.7 and 374.6 eV) were observed in DENAgNPs-NFC film (Film B). The appearance of these peaks, which come from amine groups in dendrimer and silver particle, indicates that DENAgNPs were attached onto NFC in the nanocomposite film [32–34].

3.2. Catalytic properties of DENAgNPs-NFC films

The catalytic properties of DENAgNPs-NFC films on the decoloration of Rhodamine B were investigated in the presence of $NaBH_4$. UV–visible absorption spectra of Rhodamine B catalyzed by DENAgNPs-NFC films are presented in Fig. S6 in Appendix A. In the absence of DENAgNPs-NFC films, the color of Rhodamine B in a $NaBH_4$ solution remained invariant even for one day, and NFC film (Film A) also did not have any catalytic efficiency. Because reduced Rhodamine B is colorless, a decrease in the absorbance of Rhodamine B reveals that the dye was reduced by $NaBH_4$ in

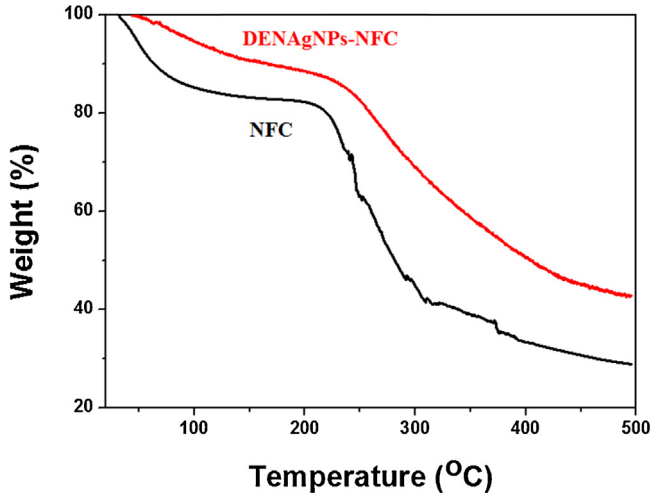

Fig. 4. Variation of mass with temperature during the thermogravimetric analysis of NFC (Film A) and DENAgNPs-NFC (Film B) films.

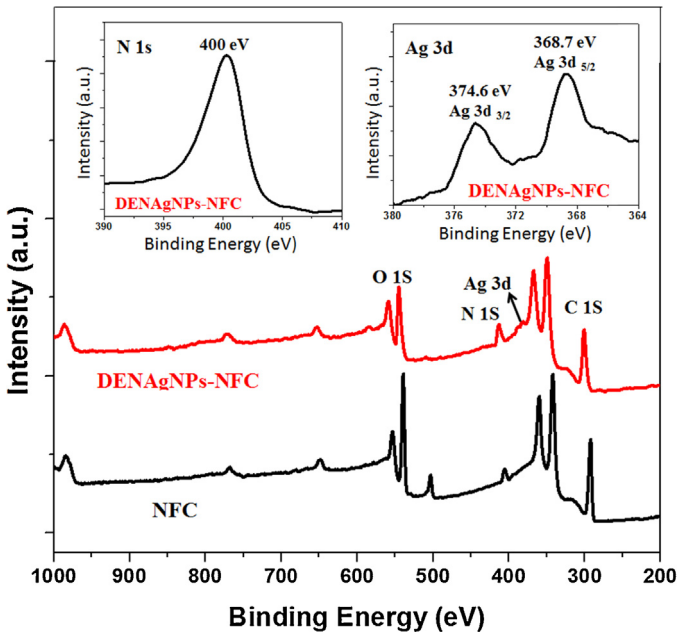

Fig. 5. XPS of NFC (Film A) and DENAgNPs-NFC (Film B) films.

the presence of catalytically performing AgNPs, as the process was happened only on Films B, C and D.

The curves of Rhodamine B concentration versus reaction time are shown in Fig. 6a. The concentration of dye was determined through a calibration curve. The concentration in the presence of Films B, C, and D decreased with time up to 30–50 min, although it depends on film. Supposing that the decomposition of Rhodamine B obeys a pseudo-first order kinetic law, $\ln(C/C_0) = k_{app}t$, where C is the concentration of Rhodamine B at time t, C_0 is an initial concentration of Rhodamine B and k_{app} is the apparent rate constant for the process [35]. The obtained decay kinetics profiles of Rhodamine B (Fig. 6b) indicated that the increase in concentration of DENAgNPs led to the significant increase in the catalytic activity. The catalytic efficiency was high, when the film surface was modified by pricking with needle. The created small holes on the film might increase the surface area and the reaction site.

The catalytic mechanism could be explained as follows. In general, Rhodamine B is electrophilic and BH_4^- is nucleophilic with respect to AgNPs. The nucleophile BH_4^- can donate electrons to AgNPs, and the electrophile Rhodamine B can capture electrons from the AgNPs. Thus, AgNPs can serve as a catalytic electron relay for the redox reduction degradation of Rhodamine B in a $NaBH_4$ solution [35,36]. Jiang et al. [37] explained the mechanism on the basis of the change in Fermi level of the supported metal particles during the catalytic process. Without metal nanoparticles, potential difference between BH_4^- and dye is too high and there is no electron transition. After the addition of AgNPs, Fermi potential of the metal particles decreases, the potential difference of BH_4^- and dye diminishes, and hence the electron transfer may occur easy through AgNPs. Meanwhile, the coexistence of dendrimer in the catalytic system may accelerate the catalytic reaction: Ag catalyst-coating dendrimer can play a role as an adsorbent and a reservoir of guest molecule to increase its number on the surface of catalyst [38–40]. The schematic mechanism is shown in Fig. 7.

3.3. Antibacterial action of DENAgNPs-NFC films

Antibacterial tests for DENAgNPs-NFC films were performed against Gram-negative (*E. coli*) and Gram-positive (*S. aureus*) bacteria. Fig. 8 shows results for antibacterial activity of Films A, A*

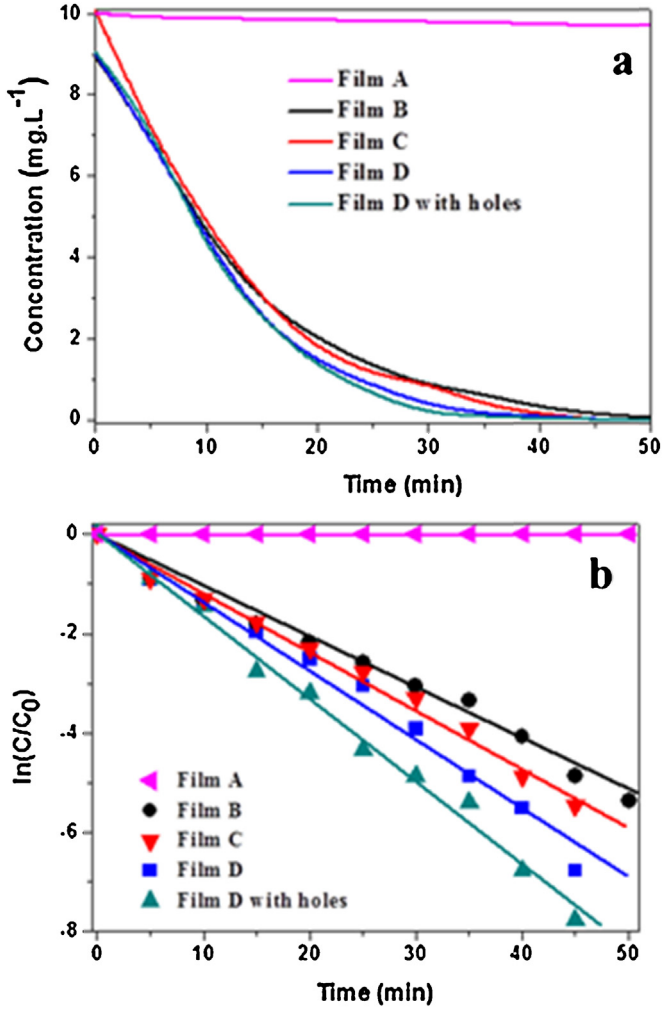

Fig. 6. (a) Curves of Rhodamine B concentration versus reaction time and (b) decay kinetics profiles of Rhodamine B in existence of NFC (Film A) and DENAgNPs-NFC (Film B–D) films (calculated from Fig. S6 in Appendix A).

(DEN-NFC), B, C and D toward Gram-negative and Gram-positive bacteria. No clear inhibition zone was observed for Films A and A*, where AgNPs were absent. However, the clear inhibition zone was visualized for films including AgNPs, indicating the sterilization of bacteria. Then the obtained data (Fig. 8) elucidated that the increase in the amount of AgNPs raised the significant increase in the antibacterial activity. Inhibition zones of 12 and 17 mm on Film D were observed for *E. coli* and *S. aureus*, respectively. Therefore, it can be noticed that Gram-positive bacteria shows higher inhibition zone than Gram-negative bacteria. The reason may be that Gram-negative bacteria are more resistant against antibodies because of

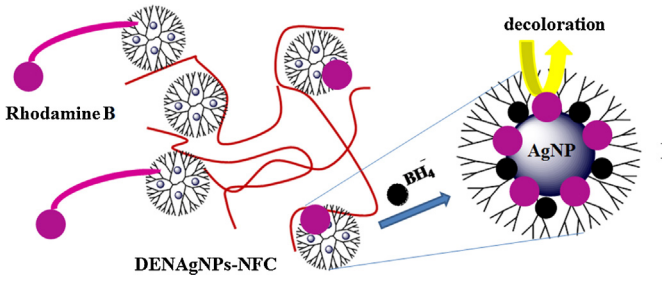

Fig. 7. Schematic mechanism of decoloration of Rhodamine B by $NaBH_4$ in the presence of DENAgNPs-NFC film.

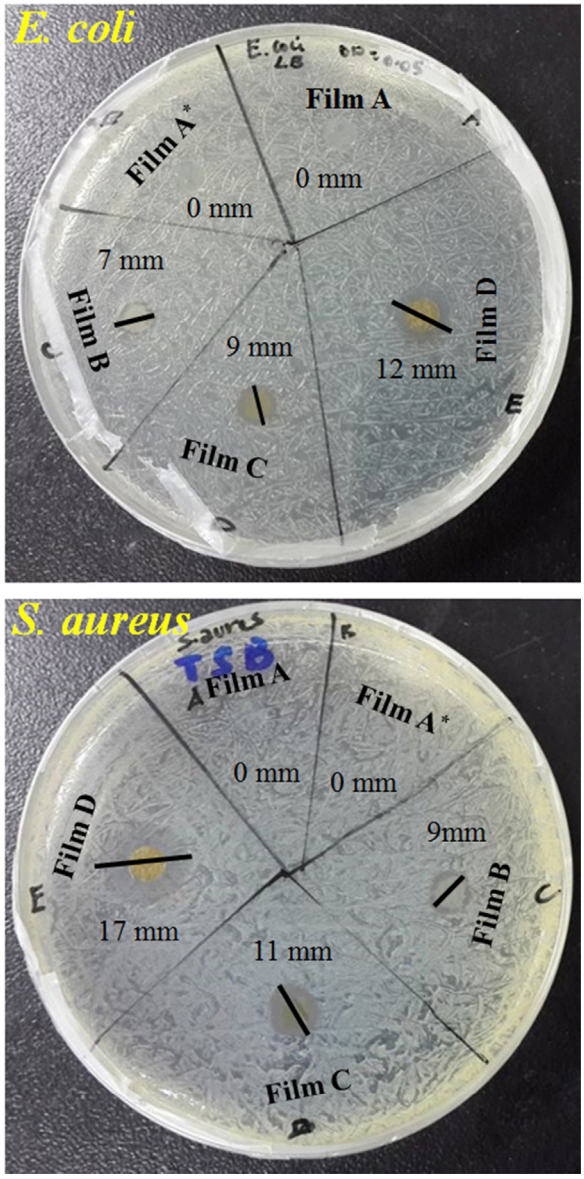

Fig. 8. Antibacterial activity of NFC (Film A), DEN-NFC (Film A*) and DENAgNPs-NFC (Film B–D) films against *Escherichia coli* and *Staphylococcus aureus*.

their impenetrability for thick cell wall than Gram-positive bacteria [41,42].

Although the inhibition mechanism by silver for bacterial growth is not necessarily clear yet, one scientific approach is relied on the assumption that silver ions (Ag^+) are released from AgNPs by reacting with oxygen and water and diffused nearby (Eq. (1)).

$$Ag + O_2 + 4H_3O^+ \rightarrow Ag^+ + 6H_2O \quad (1)$$

Then oxygen may be provided from dendrimer, because PAMAM dendrimer can encapsulate oxygen [43,44]. Both AgNPs and silver ions should be a bactericide. It might be expected that silver ions are ready to react with proteins with thiol groups (—SH) in the bacteria cell wall. Monovalent silver ions (Ag^+) would replace hydrogen ions (H^+) of sulfhydryl or thiol groups, inactivating the protein, decreasing membrane permeability, and eventually causing cellular death [41,42], although this mechanism is different from the case of bacteria inactivation on $Ag/AgBr/TiO_2$ nanotube array [45]. Moreover, if AgNPs or DENAgNPs can enter into the interior of the bacteria cell through cell membrane and react with phosphorous-containing compounds such as DNA, DNA suffers damage by the

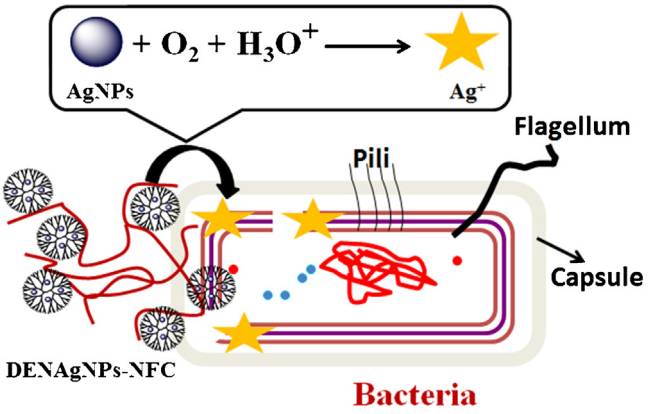

Fig. 9. Schematic mechanism of bacterial cell lysis by AgNPs.

attack of AgNPs, which adversely affects the cell division process or the respiratory chain (ATP synthesis path), leading to cell death [46,47]. The assumed mechanism of the bacterial cell lysis is schematically represented in Fig. 9.

4. Conclusions

In summary, the new and facile approach presented here supports the advantages of the DENAgNP-NFC films. The straight forward methodology can be used to guide the assembly of any combination of metallic NPs. The hybridization of AgNPs on NFC was performed using chemical (covalent) binding by mediation of dendrimer. Thus the chemical immobilization of pre-prepared DENAgNPs on NFC can offer preferable nanocomposite materials loading very stable and homogeneously distributed metal nanoparticles on the NFC. The DENAgNP-NFC films showed high catalytic activity toward the decoloration and antibacterial performance against both Gram-positive and Gram-negative bacteria, while AgNPs-free NFC films had no catalytic and antibacterial activities. Thus, this novel concept preparing film-type reactive nanocomposites demonstrates the potential to fabricate eco-friendly films having both catalytic and antibacterial activities with a good selectivity and minimizes the secondary pollutants.

Acknowledgments

This subject was financially supported by National Taiwan University of Science and Technology, Taiwan (103H237003). B.R. gratefully acknowledges National Taiwan University of Science and Technology, Taiwan, for the financial support by Postdoctoral Fellowship. We thank Prof. Cheng-Kang Lee and Prof. Masaki Ujihara of National Taiwan University of Science and Technology, Taiwan, for their valuable discussion.

Appendix A. Supplementary data

Supplementary data associated with this article can be found, in the online version, at http://dx.doi.org/10.1016/j.apcata.2014.12.045.

References

[1] I.A. Alaton, I.A. Balcioglu, J. Photochem. Photobiol. 141 (2001) 247–254.
[2] A.A. Bergwerff, P. Scherpenisee, J. Chromatogr. B 788 (2003) 351–359.
[3] Y. Kobayashi, T. Nakanishi, J. Komiyama, Text. Res. J. 72 (2002) 125–131.
[4] R. Bagherzadeh, M. Montazer, M. Latifi, M. Sheikhzadeh, M. Sattari, Fibers Polym. 8 (2007) 386–392.
[5] X. Wang, B. Ding, J. Yu, M. Wang, Nano Today 6 (2011) 510–530.
[6] D. Klemm, F. Kramer, S. Moritz, T. Lindstrom, M. Ankerfors, D. Gray, A. Dorris, Angew. Chem. Int. Ed. 50 (2011) 5438–5466.
[7] A.A. Hebeish, M.H. El-Rafie, F.A. Abdel-Mohdy, E.S. Abdel-Halim, H.E. Emam, Carbohydr. Polym. 82 (2010) 933–941.
[8] R.J. Moon, A. Martini, J. Nairn, J. Simonsen, J. Youngblood, Chem. Soc. Rev. 40 (2011) 3941–3994.
[9] M.A.S.A. Samir, F. Alloin, A. Dufresne, Biomacromolecules 6 (2005) 612–626.
[10] S.J. Eichhorn, A. Dufresne, M. Aranguren, N.E. Marcovich, J.R. Capadona, S.J. Rowan, C. Weder, W. Thielemans, M. Roman, S. Renneckar, W. Gindl, S. Veigel, J. Keckes, H. Yano, K. Abe, M. Nogi, A.N. Nakagaito, A. Mangalam, J. Simonsen, A.S. Benight, A. Bismarck, L.A. Berglund, T. Peijs, J. Mater. Sci. 45 (2010) 1–33.
[11] S. Padalkar, J. Capadona, S. Rowan, C. Weder, R. Moon, L. Stanciu, J. Mater. Sci. 46 (2011) 5672–5679.
[12] T. Nypelo, H. Pynnönen, M. Osterberg, J. Paltakari, J. Laine, Cellulose 19 (2012) 779–792.
[13] N.C.T. Martins, C.S.R. Freire, R.J.B. Pinto, S.C.M. Fernandes, C.P. Neto, A.J.D. Silvestre, J. Causio, G. Baldi, P. Sadocco, T. Trindade, Cellulose 19 (2012) 1425–1436.
[14] R.J.B. Pinto, P.A.A.P. Marques, M.A. Martins, C.P. Neto, T. Trindade, J. Colloid Interface Sci. 312 (2007) 506–512.
[15] M. Sureshkumar, D.Y. Siswanto, C.K. Lee, J. Mater. Chem. 20 (2010) 6948–6955.
[16] L. Shang, B. Li, W. Dong, B. Chen, C. Li, W. Tang, G. Wang, J. Wu, Y. Ying, J. Hazard. Mater. 178 (2010) 1109–1114.
[17] Y. Zhang, Z.R. Tang, X. Fu, Y. Xu, ACS Nano 4 (2010) 7303–7314.
[18] L. Liu, H. Bai, J. Liu, D.D. Sun, J. Hazard. Mater. 261 (2013) 214–223.
[19] H.R. Pant, D.R. Pandeya, K.T. Nam, W.I. Baek, S.T. Hong, H.Y. Kim, J. Hazard. Mater. 189 (2011) 465–471.
[20] H.R. Pant, B. Pant, P. Pokharel, H.J. Kim, L.D. Tijing, C.H. Park, D.S. Lee, H.Y. Kim, C.S. Kim, J. Membr. Sci. 429 (2013) 225–234.
[21] B. Ramaraju, T. Imae, RSC Adv. 3 (2013) 16279–16282.
[22] A. Manna, T. Imae, K. Aoi, M. Okada, T. Yogo, Chem. Mater. 13 (2001) 1674–1681.
[23] T. Yamazaki, T. Imae, J. Nanosci. Nanotechnol. 5 (2005) 1066–1071.
[24] T. Yamazaki, T. Imae, H. Sugimura, N. Saito, K. Hayashi, O. Takai, J. Nanosci. Nanotechnol. 5 (2005) 1792–1800.
[25] T. Imae, S. Hamaguchi, Carbohydr. Polym. 88 (2012) 352–360.
[26] R.C. Sun, C.F. Liu, J.L. Ren, F. Xu, J.J. Liu, J.X. Sun, J. Agric. Food Chem. 54 (2006) 5742–5748.
[27] J. Lu, P. Askeland, L.T. Drzal, Polymer 49 (2008) 1285–1296.
[28] C.C. Wagner, E.G. Ferrer, E.J. Baran, Acta Farrtz. Bonaeretise 18 (1999) 5–12.
[29] K.N. Han, B.Y. Yu, S.Y. Kwak, J. Membr. Sci. 396 (2012) 83–91.
[30] M. Ito, T. Imae, K. Aoi, K. Tsutsumiuchi, H. Noda, M. Okada, Langmuir 18 (2002) 9757–9764.
[31] M. Ito, T. Imae, J. Nanosci. Nanotechnol. 6 (2006) 1667–1672.
[32] Z. Zhang, C. Shao, Y. Sun, J. Mu, M. Zhang, P. Zhang, Z. Guo, P. Liang, C. Wang, Y. Liu, J. Mater. Chem. 22 (2012) 1387–1395.
[33] T. Wu, X. Wang, H. Qiu, J. Gao, W. Wang, Y. Liu, J. Mater. Chem. 22 (2012) 4772–4779.
[34] R.C. Gamez, E.T. Castellana, D.H. Russell, Langmuir 29 (2013) 6502–6507.
[35] C. An, J. Wang, W. Jiang, M. Zhang, X. Ming, S. Wang, Q. Zhang, Nanoscale 4 (2012) 5646–5650.
[36] W.W. He, X.C. Wu, J.B. Liu, K. Zhang, W.G. Chu, L.L. Feng, X.A. Hu, W.Y. Zbou, S.S. Me, J. Phys. Chem. C 113 (2009) 10505–10510.
[37] Z. Jiang, C. Liu, L. Sun, J. Phys. Chem. B 109 (2005) 1730–1735.
[38] Y. Nakanishi, T. Imae, J. Colloid Interface Sci. 285 (2005) 158–162.
[39] Y. Nakanishi, T. Imae, J. Colloid Interface Sci. 297 (2006) 122–129.
[40] B. Krishnakumar, T. Imae, Appl. Catal. A: Gen. 486 (2014) 170–175.
[41] J.S. Hoskins, T. Karanfil, S.M. Serkiz, Environ. Sci. Technol. 36 (2002) 784–789.
[42] C. Damm, H. Muenstedt, A. Roesh, J. Mater. Sci. 42 (2007) 6067–6073.
[43] C.-C. Chu, T. Imae, Macromol. Rapid Commun. 30 (2009) 89–93.
[44] G. Saravanan, T. Imae, J. Nanosci. Nanochem. 11 (2011) 4838–4845.
[45] Y. Hou, X. Li, Q. Zhao, G. Chen, C.L. Raston, Environ. Sci. Technol. 46 (2012) 4042–4050.
[46] J.S. Kim, J. Ind. Eng. Chem. 13 (2007) 718–722.
[47] Z. Xiu, Q. Zhang, H.L. Puppala, V.L. Colvin, P.J.J. Alvarez, Nano Lett. 12 (2012) 4271–4275.